Research Article Open Access

Miroslava Nedyalkova*, Vladislav Antonov

Manganese oxalates - structure-based Insights

https://doi.org/10.1515/chem-2018-0123
received June 8, 2018; accepted August 8, 2018.

Abstract: We have investigated the crystal and magnetic structures of α -$MnC_2O_4 \cdot 2H_2O$ and γ-$MnC_2O_4 \cdot 2H_2O$ by the frame of density functional theory calculations and the augmented plane wave approach as implemented in the WIEN2k code. We also present a generally applicable approach step-wise dehydration process of $MnC_2O_4 \cdot 3H_2O$ based on molecular dynamic simulations. Also, first principles calculations of NMR parameters along with the magnetic susceptibility were performed to reveal new insights into a quite exotic behavior which hampered the experimental way once by the domination of large paramagnetic shift of the d-electrons. The proposed approach paves the way for setting possible widenings by the implementation of computational strategies for such type of systems.

Keywords: Mn oxalates; magnetic; antiferromagnetic; hydrate; NMR.

1 Introduction

Manganese oxalate draws the interest for a long time because may be used as precursors for obtaining of oxide systems and oxide particles with specified stoichiometric composition and crystallite size, for obtaining metal phase, etc.[1–4]. The structure investigations of some manganese oxalates like for example α′- and α″-modifications of $MnC_2O_4 \cdot 2H_2O$ are reported in the literature in the work of Deyrieux et al. [5]. The common ordering type resembling one-dimensional infinite chains of Mn-oxalate is observed in both alfa forms. The manganese atom is coordinated with the two chelate oxalates in equatorial plane and two water molecules in axial positions. The structure of γ- $MnC_2O_4 \cdot 2H_2O$ [6] corresponds to the modification predicted by Huizing [7] in which each Mn atom in the one-dimensional chains is bounded with one chelate oxalate and two bridged oxalates in the equatorial plane, and two water molecules in axial positions. Pezerat et al. [8] have described the partial structure of α-$MnC_2O_4 \cdot 2H_2O$ as equivalent to humboldtine FeC_2O_4. The structure of $MnC_2O_4 \cdot 3H_2O$ is described by Fu et al. [9]. Based on the presented state-of-the-art the overall deliberation about the manganese oxalates data is insufficient especially in the light of structure and magnetic features and NMR.

NMR data from ^{55}Mn oxalates are currently scarce in the literature, both experimentally and computational. The quadrupoles are the most NMR active transition metal nuclei; the problem is the non-integer spin and typically yields to wide-ranging NMR powder patterns in the solid state. The magnetic shielding tensor is key factor encompasses information regarding local molecular–electronic structure.

Here, we demondstrate results relies on structure-magnetic properties of manganese oxalate hydrates in alfa and gamma forms and step-wise dehydration process for obtaining the anhydrate of $MnC_2O_4 \cdot 3H_2O$ in the frame of ab initio and molecular dynamic calculations. Herein the presented calculated data for predicted magnetic shielding is based on a first-principles calculation of using a full potential linearized augmented plane wave based (FP-LAPW) method based on the DFT, implemented in the WIEN2k package [10].

2 Experimental

2.1 Computational details for the full-potential linear augmented plane-wave (FP-LAPW) calculations

The WIEN2k calculations performed in this work are based on full-potential linearized augmented plane wave (FP-LAPW) method, which is known to be the most exact one for electronic structure calculation of periodic compounds. The standard augmented plane wave basis set is extended with eight additional local orbitals (NMR-

***Corresponding author: Miroslava Nedyalkova,** Chair of General and Inorganic Chemistry, Faculty of Chemistry and Pharmacy, University of Sofia "St. Kl. Okhridski", J. Bourchier Blvd. 1, 1164 Sofia, Bulgaria, E-mail: mici345@yahoo.com
Vladislav Antonov: Chair of Nuclear Research and Nuclear Energy, Bulgarian Academy of Sciences, Acad. G. Bonchev str., bl.11, Sofia-1113, Bulgaria

LOs) at higher expansion energies for all "chemical" l + 1 angular moment. The Greens function used to indicate the perturbation of the ground state is augmented with extra terms to accelerate convergence concerning the number of NMRLOs. The splitting of the valence and core states significantly changes the absolute values of the shielding; thus in the present sudy, the corresponding core-correction is conducted. All molecular calculations are completed with the 1s state as the core for all atoms (except H) because of the short bond-lengths in these molecules, while for the bulk calculations we applied the usual WIEN2k criterion defining valence states as states with atomic eigenvalues above −6 Ry. The numerical parameters are set to the standard WIEN2k scheme. The convergence concerning the basis set size (RKMAX) has been tested, and the presented values of the shielding for the molecular systems are extrapolated to infinite RKMAX (1-3 ppm compared to the largest applied RKMAX). The computational protocol is tested and presented for other wien2k users as well. The generalized gradient approximation (GGA) of Perdew–Burke–Ernzerhof for the exchange–correlation functional [11] is applied. The muffin tin sphere radii (RMT) value for Mn atom was taken to be 1.87 a.u. and 100 k-points were used over the irreducible part of the first Brillouin zone (IBZ).

2.2 Molecule dynamics

Dehydration process of $MnC_2O_4 \cdot 3H_2O$ is a dynamical occurrence, and although the study of crystal structures can be an insightful example for the dynamic phenomena beyond the static crystal structure and to shed of light on these processes. The molecular dynamics (MD) simulations have been applied for proving the ability of dynamic characteristic for materials descriptions at the atomic level. MD simulations have been successfully used to study different problems, starting from protein folding, drug modelling, conformational reorganizations of molecules and their interactions with other molecules and many more [12-14]. Implementation of MD simulations to organic crystal structures have been quite restricted. The basis of MD derives from Newtonian mechanics, which can calculate the time evolution of a system by integration of Newton's laws of motion. The simulation super cell will normally have side lengths of 30-100 Å.

A crystal of such size will be led by surface effect and therefore be a poor model of macroscopic ones. The water leaving mechanism of from a crystal is a complex process concerning a diffusion process. The important point and factor for dehydration is a temperature. From a modeling perspective, both these factors influence the chemical potential of the water molecules and affect the model by destabilization of the chemical potential.

Ethical approval: The conducted research is not related to either human or animal use.

3 Results and discussion

3.1 Crystal structure of α - $MnC_2O_4.2H_2O$

α - $MnC_2O_4.2H_2O$ is a one-dimensional structure (illustrated in Fig. 1 a), b) and c), with chains of oxalate-bridged manganese centers running along the c direction. Manganese is confirmed as 2^+ by bond valence sums (sum 2.06), and exists in distorted octahedral coordination, with the smallest angle (78.0 – **calculated value)**. The Mn is axially allied to two water molecules. The four manganese coordination sites are occupied by oxalate oxygen atoms. The O is three coordinate, bonded to C and two Mn(1) atoms. The oxygen O(5) positioned like terminal is linked to C(2), although the bond distance is not significantly shorter than those of the distance O(2) and O(4). All oxalate anions are equivalent and display bi- and bismonodentate coordination to manganese. Over the three coordinate O(1), manganese octahedral share bends to form chains along the c-axis along the molecule. These

Table 1: Selected bond lengths (A°) for α - $MnC_2O_4.2H_2O$.

SELECTED BOND LENGTHS (A°)			
Mn(1) O(1) 2.124606	C(1) O(1) 1.29063		
Mn(1) O(2) 2.124606	C(2) O(2) 1.29063		
Mn(1) O(5) 2.102123	C(2) O(5) 1.28702		
Mn(1) O(6) 2.102123	C(1) C(2) 1.50266		
Mn(1) O(10) 2.01709			
Mn(1) O(11) 2.01709			

Table 2: Atomic coordinates for α - $MnC_2O_4.2H_2O$.

ATOM	X	Y	Z
Mn1	0.250	0.5000	0.6182
O1	0.0780	0.32651	0.6067
O2	0.1780	0.67623	0.7660
O3	0.854	0.33370	0.51370
O4	0.000	0.00592	0.25000
C1	-0.0189	0.40552	0.5334
H1	0.2460	0.69501	0.8388
H2	0.1198	0.80520	0.75803
H3	0.0284	0.09225	0.6798

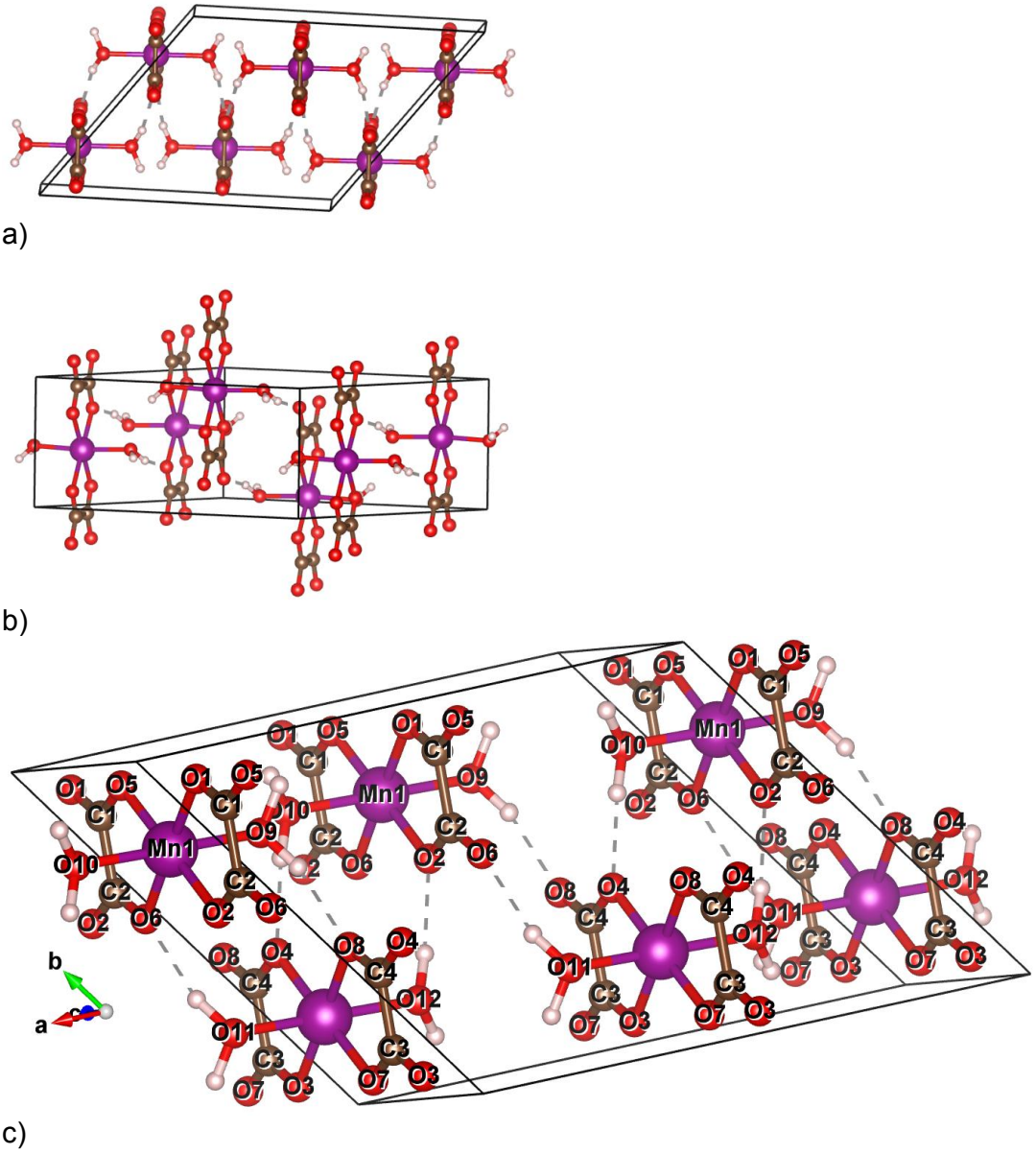

Figure 1: Molecular structure of a α - MnC2O4.2H2O: a) on top view; b) side view c) numbering.

chains pack together in two orientations in a herringbone pattern, the coordinated water molecules of neighboring chains are found a closet. Using a force minimization method in the Wien2k code, the atom positions are optimized. Optimized structural parameters (a, b, c in Å) are presented in Table 2.

3.2 Magnetic structure

Ferromagnetic (FM) and antiferromagnetic (AFM) total energies were performed to study the magnetic properties and to determine the ground state of both DMSs. In the case of the FM state, we considered the same spin direction of Mn cations and antiparallel spin in the AFM state.

Ferromagnetic (FM) and antiferromagnetic (AFM) total energies were performed to study the magnetic properties and to determine the ground state of both DMSs. In the case of the FM state, we considered the same spin direction of Mn cations and antiparallel spin in the AFM state.

Ferromagnetic (FM) and antiferromagnetic (AFM) total energies calculations were performed. In the case of the FM state, we considered the same spin direction of Mn cations and antiparallel spin in the AFM state.

It should be noted that considering the conclusions in the article [15] it can be expected that addition of water in the manganese oxalate leads to non-collinear magnetism due to additional magnetic exchange interactions through the water molecules. The nature of this phenomena is not yet to be explained and requires experimental studies like neutron diffraction. However, this non-collinear magnetization requires extended crystal cells for computations which could be beyond the available computational resources. Though, estimations could be made when smaller magnetic components which are neglected, and collinear magnetic setup is used. The theoretical calculations based on spin-orbital energy calculations predict the observed magnetic structure corresponds to the antiferromagnetic state. An antiferromagnetic ordering occurs with the magnetic unit cell equivalent to the crystalline unit cell. Hence there is a possibility of superexchange antiferromagnetic interaction between oxygen p_x and p_y states with Mn1/ Mn2 d-states between the layer. As a result, one could expect AFM interaction between the layers and FM interaction within the layer leading to AFM order. Our total energy calculations also show that the AFM ordering is the lowest energy configuration in this system. The theoretical finding of AFM ordering in the α-$MnC_2O_4.2H_2O$ could also support the theoretical obtained negative value from the susceptibility (Magnetic Susceptibility (total) [10^{-6} cm^3 mol^{-1} $cell^{-1}$]=-69.114), if we have an experimental measurements Curie temperature this will be the second proof for the AFM order. For evaluation we are providing the data for magnetic ordering in α-Mn_2O_3 has been studied by neutron powder diffraction measurements and the ordering has been proven as well antiferromagnetic [16].

3.3 Crysral structure of γ-$MnC_2O_4{\cdot}2H_2O$

The six oxygens from oxalate ion are coordinated with Mn. Herewith three oxalate ions are bonded with Mn atom via one oxygen atom and two oxalates form the chelate bonds including two oxygens (Figure 2a,b)

The Mn atoms are in special position on the mirror plane. The presented in the literature [17] structure data does not give the positions of the H atoms. The initial guess for their positions was made, and atomic relaxation was made. The structure was idnetified using ISOTROPY code [18] as Orthorhombic, P212121 with the following parameters given in table 3 and 4.

Table 3: Selected bond lengths (A°) for g- $MnC_2O_4.2H_2O$.

SELECTED BOND LENGTHS (A°)
Mn(1) O(1) 2.271
Mn(1) O(2) 2.153
Mn(1) O(2) 2.153
Mn(1) O(4) 2.161
Mn(1) O(5) 2.228
Mn(1) O(6) 2.164

Table 4: Atomic coordinates for g- $MnC_2O_4.2H_2O$.

ATOM	X	Y	Z
Mn1	0.810	0.921	0.4280
O1	0.799	0.940	0.058
O2	0.901	0.781	0.283
O3	0 .888	0.688	- 0.011
O4	0.854	0.855	-0.252
O5	0.474	0.867	0.427
O6	1.121	0.990	0.422
C1	0.842	0.861	-0.049
C2	0.881	0.768	0.088
H1	0.066	0.157	0.744
H2	0.056	0.195	0.050

3.4 Magnetic structure

To refine the results for the magnetic structure, the axis of the collinear magnetization was changed to x and y. The magnetic moments tend to be ferromagnetically coupled in an x-y plane for the case of gamma oxalate. Also, the value of the magnetic susceptibility (χ) obtained by NMR calculations is 4.8, which leads the magnetic moment of 6.21μ_B expected for the weak ferro magnetically ordered Mn.

The observed results and for both Mn oxalates are a specific label for high spin Mn^{2+} ions with S= 5/2. If the same state of observation could be obtained through the non-collinear orientation of in the staring ground state calculations by the neighboring spins whose interaction is antiferromagnetic and is a result from the exchange over the oxalate bridges modified with additional perturbations (usually antisymmetric operations) which favor the canting of the neighboring spins. These spins are canted toward the applied magnetic field easier than in the antiferromagnets. This phenomenon deserves a further study of the magnetic structure, since in a similar Mn-networks if we can label the whole structure, the true antiferromagnetic was observed. In the magnetic

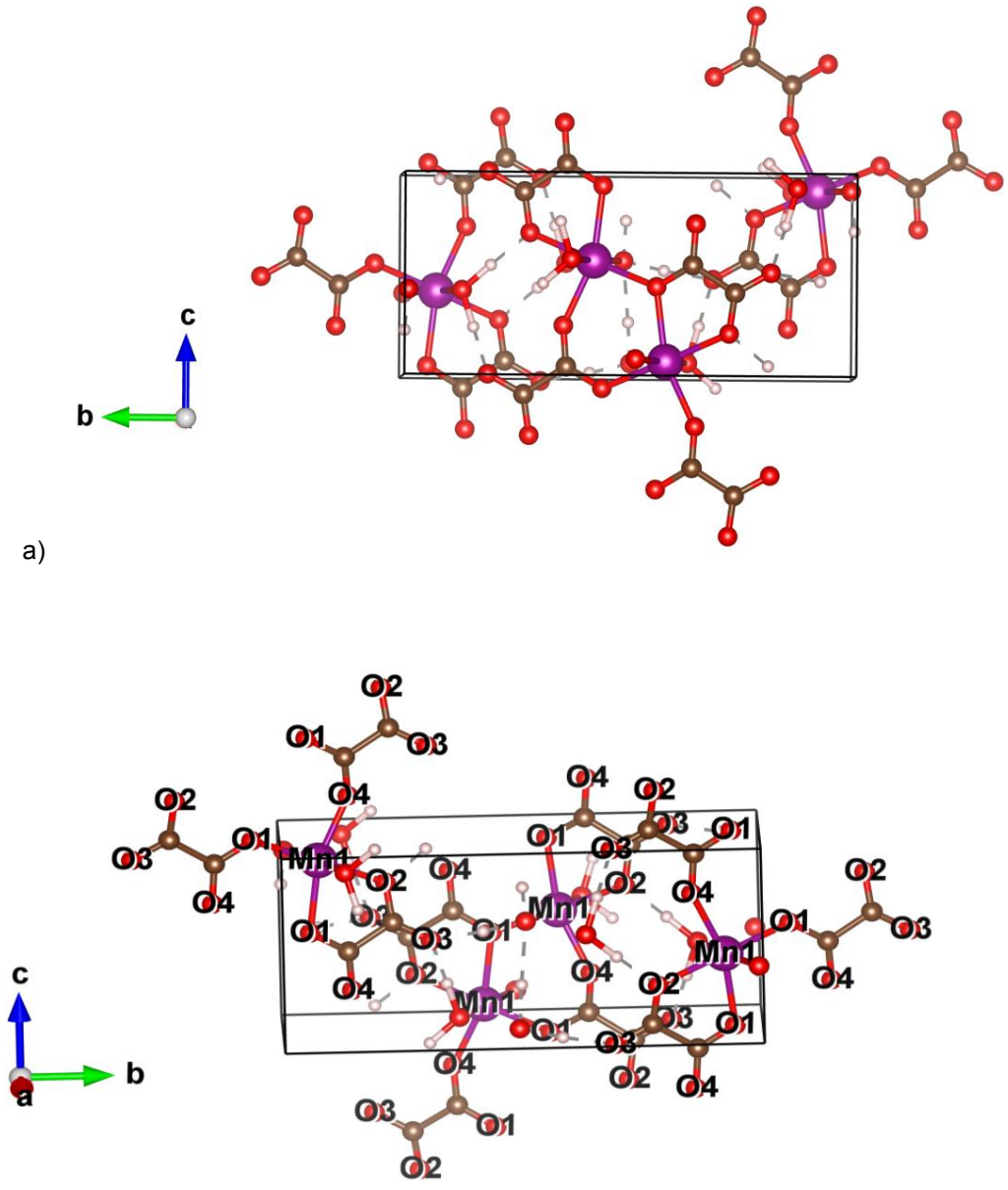

Figure 2: Molecular structure of g- $MnC_2O_4.2H_2O$: a) side view b) numbering.

ground state in the ordered framework can be described as an antiferromagnetic-like network of slightly canted Mn^{2+} spins with the contribution of the incorporated paramagnetic terms. The more complicated structures like the pointed out here the presence of many non-trivial terms marks the quantitative description of the weak ferromagnetic structure not so easy, and further experimental investigation and advanced modelling will be required to address this question.

3.5 Analysis of 55Mn NMR spectra of in α-$MnC_2O_4.2H_2O$ and γ-$MnC_2O_4\cdot2H_2O$

Predicting NMR properties by computational tools is a valuable tool to assist the experimentalists in the characterization of molecular structure [19-22].

Solid-state NMR calculations based on DFT have been used to examine the NMR shielding in α-$MnC_2O_4.2H_2O$. The parameters obtained from simulations of the central transition ^{55}Mn NMR and ^{13}C spectra with Wien2k and also for comparison with gauge-including projector

Table 5: Wien2k and GIPAW NMR data.

CODE	D^{ISO} – ^{55}MN ALFA	D^{ISO} – ^{13}C ALFA	D^{ISO} – ^{55}MN GAMA	D^{ISO} – ^{13}C GAMA
WIEN2K	-1765 ppm	168.9	-7075 ppm	168.5 ppm
GIPAW	-2245 ppm	168.1	NA	168.6 ppm

augmented-wave (GIPAW) method [23-25] using the Quantum Espresso Code are tabulated below.

The isotropic chemical shift δ^{iso} is defined as $\delta^{iso} = -[\sigma - \sigma^{ref}]$, where σ^{iso} the isotropic shielding from calculations and σ^{ref} is the isotropic shielding of the same nucleus in a reference system, $MnCO_3$ (σ^{ref} = -2325 ppm) in the present case. To compute the chemical shifts, the calculations of the current induced by the external magnetic field should be conducted.

The paramagnetic contribution to shielding, which is normally with negative value (i.e., deshielding), is related to the magnetic dipole allowed mixing between symmetry-appropriate occupied and virtual molecular orbitals (MOs). This term is largely responsible for substituent effects on magnetic shielding. Magnetic shielding values are not referenced to the experimental isotropic shielding value in the present study. Qualitatively, the magnitude of paramagnetic contribution dependent both on the energy difference between the two MOs, and the matrix elements of the virtual and occupied orbital wave functions. The origin of large magnetic shielding anisotropy for transition metals can often be simplified by considering the energy difference splitting occupied and virtual metal d-character MOs within the framework of ligand field theory.

3.6 Step-wise mechanism of dehydration of Mn trihydrate

The crystal structure of Mn trihydrate has been optimized on ab ignition level first, starting from the experimental x-ray data file and adding missing H atoms.

The minimized structure, in theory, represents the crystal structure at 0 K and must be heated carefully to the temperature at which dehydration is to be simulated. Heating the crystal structure should be step-wise, the quick and shocking increasing in the temperature can tend to artefacts and quickly can potentially disorder in the structure. The different series of simulation were conducted indeed to generate new snapshots for the temperature gradient. The temperature step was 25 K, the last structure at each temperature step was used as a starting in the next step.

In the last step at 300 K, the constant number, pressure, and the temperature is performed for one ns simulation equilibrated system and more two ns for an effective run.

The timescales of MD run are not **compatible** with **experimental** timing process, for that in our scenario the water molecules are removed one often one water molecules

from the system. We choose in the case of eliminating the two water molecules to remove the surface water molecules.

The computational product results are below:

Figure 3 illustrates that the loss of waters induces a rearrangement of the structure by increasing the distance between layers, manganese ions and also changing the angels in the main unit in structure. The collapse of structure drove the next step to full dehydrated form; these results indicate the water channel (hydrogen net) hydrogen bond network allowing the alignment and order of the molecules in the order structure.

4 Conclusions

The NMR computational approach has been applied for the first time like a challenge for to first studies on the hydrated a- and g-Mn oxalates. NMR parameters extracted from calculations it helped to experimental findings. Likewise, in the light of Molecular dynamic the results that were revealed are focused in the internal water net and the absence of water molecules in the trihydrate Mn oxalates leads to unstable anhydride form.

Acknowledgements: Miroslava Nedyalkova is gratefully acknowledged for the support of DCOST 01/18 program – NSF, Bulgaria. This work was supported by the Operational Programme "Science and Education for Smart Growth 2014 - 2020" under the Project BG05M2OP001-2.009-0028. M.N is grateful for the project support: BG05M2OP001-1.001-0004/28.02.2018 (2018-2023))

Conflict of interest: Authors declare no conflict of interest.

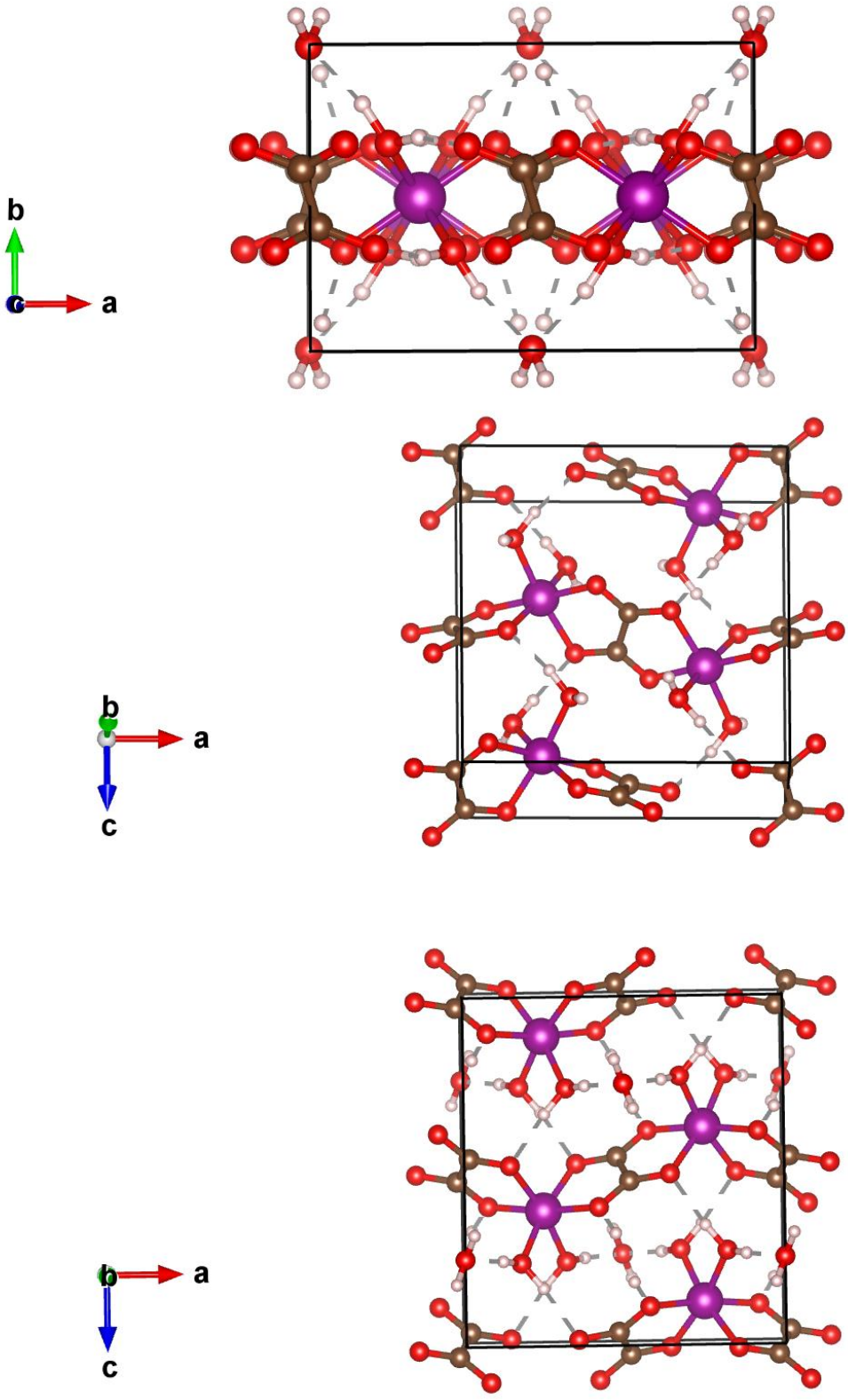

Figure 3: Water molecules distribution.

References

[1] Gydrasova I., Krasilnikov V.N., Bazuyev G.V., Synthesis of micro and nanosized manganese oxides obtained from hydrated manganese oxalates and products of their thermal modifications by ethylene glycol, J. Inorg. Chem., 2009, 54, 1097–1102.

[2] Mu J., Perlmutter D., Thermal decomposition of carbonates, carboxylates, oxalates, acetates formates, and hydroxides, Thermochim. Acta, 1981,49, 207–218.

[3] Auffrédic J.-P., Boultif A., Langford J.I, Louër D., Early stages of crystallite growth of ZnO obtained from an Oxalate precursor, J. Am. Ceram. Soc., 1995, 78, 323–328.

[4] Donkova B., Mehandjiev D., Mechanism of decomposition of manganese(II) oxalate dihydrate and manganese(II) oxalate trihydrate, Thermochimica Acta, 2004, 421, 141-149.

[5] Deyrieux R., Berro Ch., Peneloux A., Structure crystalline des oxalates dehydrates de manganese, de cobalt, de nickel et de zink, Bull. Soc. Chim. Fr., 1973, 25–34.

[6]. Lethbridge Z.A.D, Congreve A.F., Esslemont E., Slawin A.M.Z., Lightfoot P.,Synthesis and structure of three manganese oxalates: $MnC_2O_4 \cdot 2H_2O$, $[C_4H_8(NH_2)_2][Mn_2(C_2O_4)_3]$ and $Mn_2(C_2O_4)(OH)_2$, J. Solid State Chem., 2003, 172 212–218.

[7] Huizing A., van Hal H.A.M., Kwestroo W., Langereis C., van Loosdregt P.C., Hydrates of manganese (II) oxalate, Mater. Res. Bull., 1997, 12, 605–611.

[8] Pezerat H., Dubernat J., Lagier J.-P., Structure des oxalates dehydrates de magnesium, manganese, fer, cobalt, nickel et zink. Existence de faultes d'empilement, Comptes Rendus Acad. Sci. Paris, 1968, C266,1357–1360.

[9] Fu X., Wang Ch, Li M., Catena-Poly[[[diaquamanganese(II)]-μ-oxalato] monohydrate], Acta Cryst., 2005, E61, 1348–1349.

[10] Schwarz K., Blaha P., Madsen G.K.H., Electronic structure calculations of solids using the WIEN2k package for material Sciences, Comp. Phys. Commun., 2002, 147, 71-76.

[11]. Perdew J.P., Burke K., Ernzerhof M.,Generalized Gradient Approximation Made Simple, Phys. Rev. Lett., 1996, 77, 3865.

[12] Lee M.S., Salsbury F.R., Brooks C.L., Novel generalized Born methods, J. Chem. Phys., 2002, 14, 10606–10614.

[13] Mongan J., Simmerling C., McCammon J.A., Case D.A., Onufrit A., Generalized Born with a simple, robust molecular volume correction, J. Chem. Theory Comput., 2006, 3, 156–169.

[14] Lee M.S., Feig M., Salsbury F.R., Brooks C.L., New analytic approximation to the standard molecular volume definition and its application to generalized born calculations, J. Comp. Chem., 2003, 24, 1348–1356.

[15] Sledzinska I., Murasik A., Fische P., J. Phys. C: Solid State Phys., 1987, 20, 2247-2259.

[16] Wu W., Song Y., .Li Y.-Z, You Z., Heterometallic Cr–Mn Complexes Containing Cyanide and Oxalate Bridges, Inorganic Chemistry Communication, 2005, 8, 5732–736.

[17]. Regulski M., Przeniosło R., Sosnowska I., Hohlwein D., Schneider R., Neutron diffraction study of the magnetic structure of α-Mn_2O_3, Journal of Alloys and Compounds, 2004, 362, 236-240.

[18] Stokes H. T, Hatch D. M., Campbell B. J., ISOTROPY, Journal of Solid State Chemistry 2003, 172, 212–218.

[19] Al-Wahaibi L., Govindarajan M., El-Emam A., Spectroscopic (FT-IR, FT-Raman, UV, 1H and 13C NMR) insights, electronic profiling and DFT computations on ({(E)-[3-(1H-imidazol-1-yl)-1-phenylpropylidene] amino}oxy)(4nitrophenyl)methanone, an imidazole-bearing anti-Candida agent, Open Chemistry, 2018, 16, 50-63.

[20] Imutairi M., Muthu S., Prasana J., Comprehensive spectroscopic (FT-IR, FT-Raman, 1H and 13C NMR) identification and computational studies on 1-acetyl-1H-indole-2,3-dione, Open Chemistry, 2017, 15, 225-237.

[21] Al-Wabli R., Govindarajan M., Almutairi M., A combined experimental and theoretical study on vibrational and electronic properties of (5-methoxy-1H-indol-1-yl)(5-methoxy-1H-indol-2-yl)methanone, Open Chemistry, 2017, 15, 238-246.

[22] Antonov V., Nedyalkova M., Tzvetkova P., Solid State Structure Prediction Through DFT Calculations and 13C NMR Measurements: Case Study of Spiro-2,4-dithiohydantoins, Zeitschrift für Physikalische Chemie, 2015, 230, 909-930.

[23] Charpentier T., The PAW/GIPAW approach for computing NMR parameters: A new dimension added to NMR study of solids, Solid State Nuclear Magnetic Resonance, 2011, 40, 1-20

[24]. Charpentier T., Kroll P., Mauri F., An example of DFT-GIPAW in Glass science: First-Principles Nuclear Magnetic Resonance Structural Analysis of Vitreous Silica, J. Phys. Chem. C, 2009, 113, 7917-7929.

[25] Marques M., d'Avezac M., Mauri F., An example of DFT-GIPAW in nanotechnology: "Magnetic response and NMR spectra of carbon nanotubes from ab initio calculations, Phys. Rev. B, 2006, 73, 125433.